RESEARCH ARTICLE | SEPTEMBER 22 2023

Dynamics of rigid achiral magnetic microswimmers in shear-thinning fluids \odot

David Quashie, Jr. ⁽ⁱ⁾; Qi Wang ⁽ⁱ⁾; Sophie Jermyn ⁽ⁱ⁾; Jaideep Katuri ⁽ⁱ⁾; Jamel Ali ■ ⁽ⁱ⁾



Physics of Fluids 35, 092016 (2023) https://doi.org/10.1063/5.0167307





CrossMark

Articles You May Be Interested In

Completing the dark matter solutions in degenerate Kaluza-Klein theory

J. Math. Phys. (April 2019)

Gibbs measures based on 1d (an)harmonic oscillators as mean-field limits

J. Math. Phys. (April 2018)

An upper diameter bound for compact Ricci solitons with application to the Hitchin-Thorpe inequality. II

J. Math. Phys. (April 2018)



Dynamics of rigid achiral magnetic microswimmers in shear-thinning fluids

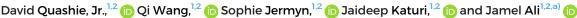
Cite as: Phys. Fluids **35**, 092016 (2023); doi: 10.1063/5.0167307 Submitted: 11 July 2023 · Accepted: 28 August 2023 · Published Online: 22 September 2023



















AFFILIATIONS

Department of Chemical and Biomedical Engineering, FAMU-FSU College of Engineering, Tallahassee, Florida 32310, USA

ABSTRACT

Here, we use magnetically driven self-assembled achiral swimmers made of two to four superparamagnetic micro-particles to provide insight into how swimming kinematics develop in complex, shear-thinning fluids. Two model shear-thinning polymer fluids are explored, where measurements of swimming dynamics reveal contrasting propulsion kinematics in shear-thinning fluids vs a Newtonian fluid. When comparing the velocity of achiral swimmers in polymer fluids to their dynamics in water, we observe kinematics dependent on (1) no shearthinning, (2) shear-thinning with negligible elasticity, and (3) shear-thinning with elasticity. At the step-out frequency, the fluidic environment's viscoelastic properties allow swimmers to propel faster than their Newtonian swimming speed, although their swimming gait remains similar. Micro-particle image velocimetry is also implemented to provide insight into how shear-thinning viscosity fluids with elasticity can modify the flow fields of the self-assembled magnetic swimmers. Our findings reveal that flow asymmetry can be created for symmetric swimmers through either the confinement effect or the Weissenberg effect. For pseudo-chiral swimmers in shear-thinning fluids, only three bead swimmers show swimming enhancement, while four bead swimmers always have a decreased step-out frequency velocity compared to their dynamics in water.

Published under an exclusive license by AIP Publishing. https://doi.org/10.1063/5.0167307

I. INTRODUCTION

Synthetic micro-scale swimmers, which propel in viscositydominated environments, have been used to optimize swimmer geometry and provide insight into swimmer interactions with complex environments, such as boundaries and viscoelastic fluids. 1-4 While commonly designed to mimic the swimming propulsion mechanisms of bacteria (helical) and sperm (flexible), alternative geometric designs, which are sometimes more efficient, have been utilized to provide additional insight into locomotion at low Reynold's number. These alternative designs can achieve driven motion through externally applied signals, such as magnetic and acoustic fields or through local, asymmetric chemical reactions at the surface of or within geometries of propellers.8

Here, we focus on the actuation of rigid, non-helical (i.e., achiral) magnetic objects using a homogeneous rotational magnetic field. Small scale, achiral magnetic structures have been of growing interest in part due to the simple manufacturing methods that can be used for fabrication, such as the random assembly of magnetic particles and traditional photolithography. 12 These structures have also been recently used to identify the optimal geometry for low Reynold's number magnetic propellers.⁵ The propulsion mechanism of these swimmers is well understood theoretically 13,14 and experimentally 11 in Newtonian fluids whether propelling near 15-17 or far from solid interfaces. These magnetic swimmers can orient to break their symmetrical dynamics resulting in the conversion of rotational motion into translational motion due to a geometric parameter called pseudo-chirality, which describes the number of geometric orientations of the swimmer that cannot be superimposed unto its mirrored image. 5,11,14

Since envisioned for biomedical applications, where propulsion will take place in biological fluids, it is necessary to understand how these viscoelastic fluids and their underlying microstructure affect the propulsion kinematics of magnetically actuated swimmers. The propulsion of non-helical magnetic objects in viscoelastic fluids increases the range of geometries that can achieve propulsion, which now includes shapes that cannot propel in Newtonian fluids because of their reciprocal motion. ^{10,18,19} For instance, an asymmetric magnetic dimer made by connecting epoxy beads with a steel wire was shown to propel in elastic fluids as a result of the elastic stress generated from the polymer's resistance to fluid shear.²⁰ In another study, while the rotation of a magnetic dumbbell consisting of spheres of varying sizes

²National High Magnetic Field Laboratory, Tallahassee, Florida 32310, USA

a) Author to whom correspondence should be addressed: jali@eng.famu.fsu.edu

had negligible propulsion in a Newtonian fluid due to their symmetry, when placed in an elastic fluid they propelled, ¹⁹ similar to recent work by Rogowski *et al.* ¹⁸ who used spherical magnetic beads as their swimmer. All mentioned groups attribute their swimmer's propulsion kinematics to non-uniform hoop stresses formed due to non-linear polymer effects when subject to curved streamlines.

Randomly assembled, magnetic, micron-sized particles forming rigid, curved, 3 and 4 bead chained assemblies have also been explored in viscoelastic fluids. When increasing the polymer concentrations of methyl cellulose, while in the dilute regime, the relationship between the driving frequency and swimmers velocity became non-linear.²¹ Additionally, the effect of polymer microstructure on the kinematics of randomly assembled microswimmers was explored; it was determined that if the bulk viscosity is kept constant, swimmers propel faster in solutions with high molecular weight polymers due to local viscoelastic effects. Furthermore, two viscoelastic effects, shearthinning viscosity and elasticity, were explored showing that they both modify swimming kinematics in distinct ways, where the 3 bead assembly has a higher velocity than the 4 bead assembly in a shearthinning fluid and the opposite behavior is observed in an elastic fluid.²² While the propulsion of non-helical magnetic swimmers in elastic fluids has been explored experimentally and theoretically, the locomotion of rigid, non-helical swimmers in shear-thinning fluids has not. This work explores how shear-thinning viscosity modifies the dynamics of self-assembled magnetic microswimmers with different geometries.

Understanding the locomotion of rigid, magnetic, achiral particle-assembled swimmers in viscoelastic fluids has been largely unexplored; hence, we first describe the magnetic swimmers in a Newtonian fluid. Using micro-rheology, we characterize two shearthinning fluids, xanthan gum and λ -DNA, to determine their averaged polymer relaxation time. Next, the dynamics of various self-assembled swimmer configurations (2, 3, and 4 bead assemblies) are described in both shear-thinning polymer fluids under similar driving magnetic frequencies and at their step-out frequencies. Here, the Reynold's number for the swimmers ranges from $\sim 10^{-5}$ to 10^{-7} using the density of the solvent, velocity of the swimmers (V_r) , average viscosity of the fluids, and diameter of the magnetic bead (l_c) . On the other hand, the Strouhal number, which compares the magnetic driving frequency to the swimming timescale $(\frac{l_c}{V_c})$, is dependent on the swimmer configuration, which ranges from 104 for symmetric swimmers in Newtonian fluids and 10³ for pseudo-chiral and symmetric swimmers in shear-thinning fluids. We then experimentally characterize the flow fields produced near magnetic swimmers, identifying how the flow field changes in water compared to the shear-thinning fluids. Finally, we propose a mechanism to explain the observed swimmer dynamics in (1) fluids with no shear-thinning, (2) fluids with shear-thinning with negligible elasticity, and (3) fluids with shear-thinning and elasticity.

II. EXPERIMENTAL METHODS

A. Fluid preparation

Xanthan Gum, XG (G1253), was purchased from Millipore Sigma (M_n : $\sim 2 \times 10^6\,\mathrm{Da}$) to create the first shear-thinning fluids. To begin, a 500 ppm XG concentration was created by adding 150 mg of XG to 300 ml of de-ionized water. The solution was then incubated at 37 °C and shaken at 300 rpm overnight to allow humectation of the

polymer molecules. The solution is then diluted to 50, 100, 200, 300, and 400 ppm and stored at $4\,^{\circ}\text{C}$ until experiments were conducted.

 Λ -DNA was also purchased from Millipore Sigma (SKU-1074572001) to create the second shear-thinning fluids. The DNA was diluted to 50 μ g/ml using TE buffer purchased from Fisher Scientific (J62388.AK). The solution was then heated at 65 °C for 10 min and further diluted to its overlap concentration²³ (c* = 40 μ g/ml). The DNA was also stained using YOYO-1 fluorescent dye purchased from Fischer Scientific (Y3601). The concentrations used for the DNA were below its overlap concentration²³ (0.4, 1, 4, 10, and 20 ppm).

B. Fluid characterization using μ -rheology

Dilute XG and DNA polymeric fluids were characterized using optical tweezer (OT) micro-rheology, probing the environment using an external force on the same length scale as the self-assembled swimmers. Probes were diluted 1:100 before adding 2 μ l of the diluted probes into 200 μ l of polymer fluids. Approximately 10 μ l of the polymer fluid with spherical probes was placed within a 0.12 mm deep, 9 mm diameter spacer (Invitrogen: S24737) secured on a 1 mm thick glass slide $(25 \times 75 \,\mathrm{mm})$ and covered with a no. 1.5 coverslip $(24 \times 50 \text{ mm})$. The chamber was then secured on the microscope equipped with a 60× water-immersion objective, a Thor labs camera (DDC1545M), and an optical force sensor.²⁴ After aligning the optical force sensor,²⁵ the objective was used to focus a 1064 nm wavelength laser to create the optical trap. OT micro-rheology was performed by oscillating five 1-µm polystyrene beads at three different locations within the sample at varying frequencies, f, in increments of 10, to determine the complex shear modulus. The imaginary complex viscosity, η'' , is determined from the loss modulus and was fitted with a multi-mode generalized linear viscoelastic Maxwell model [Eq. (1)] to determine the fluids averaged relaxation time, τ ,

$$\eta'' = \sum_{i=1}^{n} \eta''_{0,i} \cdot \exp(-\tau_i f). \tag{1}$$

C. Swimmer fabrication and actuation

Self-assembled achiral swimmers were fabricated and actuated as previously described. ^21,22 Briefly, 0.1 μ l of biotin and streptavidin magnetic beads (diameter \sim 4.45 μ m) were added to 10 μ l of DI water. The solution in gently mixed and placed next to a permanent magnet for 5 min, which causes the magnetic particles to assemble into rigid structures. The solution was then vortexed, and 300 μ l of DI water was added to the solution. Next, 2 μ l of the stock was placed in 30 μ l of the respective polymer fluids within a PDMS chamber sealed by two coverslips (Fig. 1). The sample was then placed on an inverted microscope and imaged at room temperature using a 40× objective. The magnetic swimmers (n \geq 5), which were used in these experiments, were made of 2, 3, and 4 beads.

D. Flow field analysis of self-assembled swimmers

Micro-particle image velocimetry (PIV) was used to compare the flow fields of the swimmers in water and shear-thinning fluids. A $40\times$ objective (NA 0.75) was used to capture the motion of 500 nm yellow/ green fluorescent tracer particles as the swimmers are rotated at a sampling frequency of $\sim 100\,\mathrm{Hz}$. The magnetic field strength and frequency of $14\,\mathrm{mT}$ and $30\,\mathrm{Hz}$ was left on to record the flow fields of 2, 3,

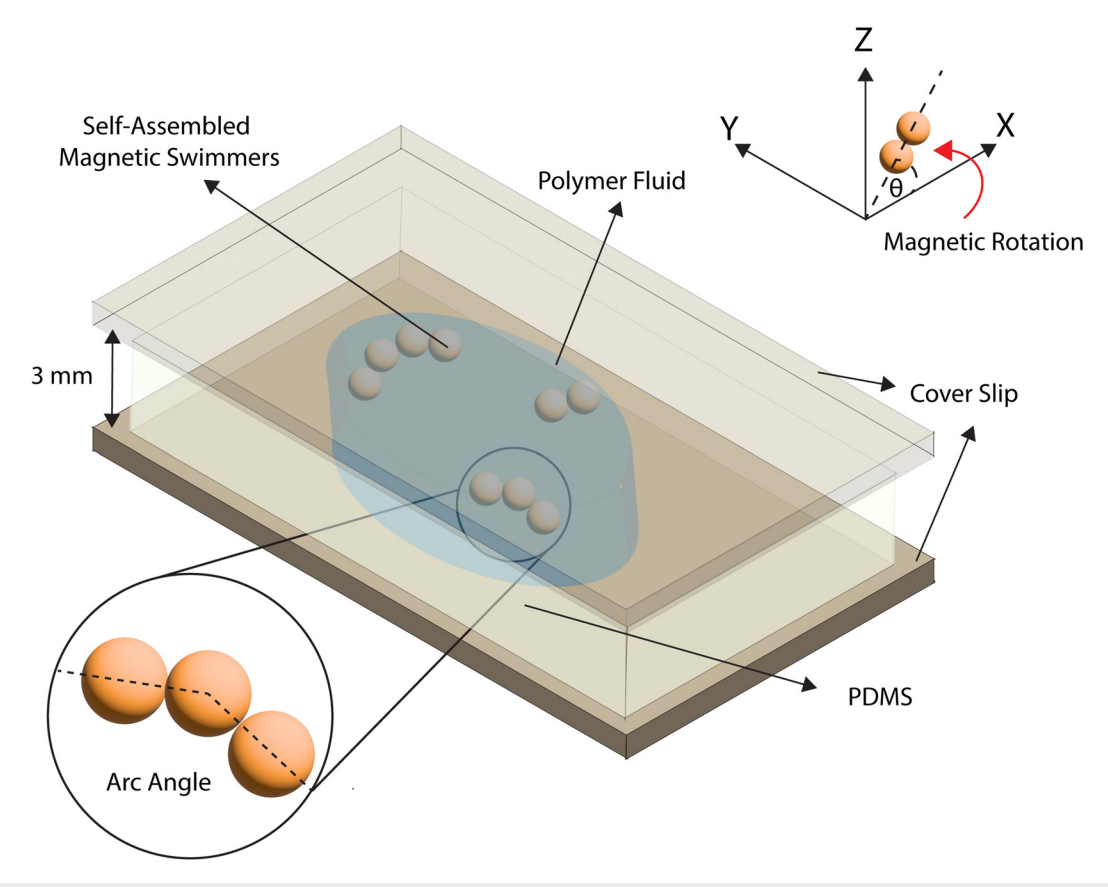


FIG. 1. Schematic of experimental chamber configuration for propulsion of self-assembled magnetic swimmers. The orientation angle, θ , of the swimmer with respect to the x-axis is shown.

and 4 bead swimmers at steady state allowing time averaging over many frames ($150 \le n \le 450$). The contrast of the videos was then enhanced and imported into LaVision DaVis 10 software for flow field analysis where the velocity's magnitude and direction were extracted. The first interrogation consisted of a window size of 32 with an overlap of 50%. The final interrogation window consisted of a window size of 12 with 4 passes and an overlap of 75%.

III. RESULTS

A. Self-assembled swimmers in water

Swimmers are fabricated through the magnetic dipole attraction of magnetized micro-particles under an external magnetic field resulting in geometries similar to that shown in Fig. 1. Swimmers are then actuated at least $100\,\mu\mathrm{m}$ from the substrate using a homogeneous magnetic field rotated along the y-z plane, resulting in the swimmers translating along the x-axis. A range of magnetic frequencies at fixed field strength (14 mT) is used to induce a magnetic torque necessary for the propulsion of the 2, 3, and 4 bead self-assembled swimmers. Briefly, at low frequencies, the swimmers rotate along an axis of symmetry resulting in cyclic motion but no lateral displacement. Eventually a critical frequency, ω_{cr} is reached where the swimmers re-orient themselves

breaking their symmetry due to their pseudo-chirality leading to propulsion. At the step-out frequency, $\omega_{\text{s-o}}$, the magnetic torque can no longer balance the fluid's resistance and, the swimmer begins to wobble. These three regimes, which have been shown experimentally ¹¹ and theoretically, ¹⁴ are observed for the three geometrical configurations of the self-assembled swimmers. We note that while a fully symmetric 2 bead swimmer cannot propel, there are minor differences in diameter for the magnetic bead causing slight displacement.

Here, the magnetic swimmers are tracked in 2D, and the displacement of the x-centroid position is used to describe the velocity of the swimmers at a range of magnetic frequencies. The velocities of the swimmers are determined from the slope, extracted from fitting the x-co-ordinate as a function of time to a linear equation, see Fig. 2(a). The 4 bead self-assembled swimmers shows the greatest displacement followed by 3 and 2 bead swimmers, which is attributed to its rotational anisotropy. The analysis of the swimmers displacement at each frequency results in a graph of velocity vs frequency where the magnetic swimmers increase their speed until the ω_{s-o} . The kinematics at the step-out frequency has been used to extract the propulsion efficiency, δ , of the swimmers [Fig. 2(b)]. The propulsion efficiency is defined as the distance covered after the swimmers complete

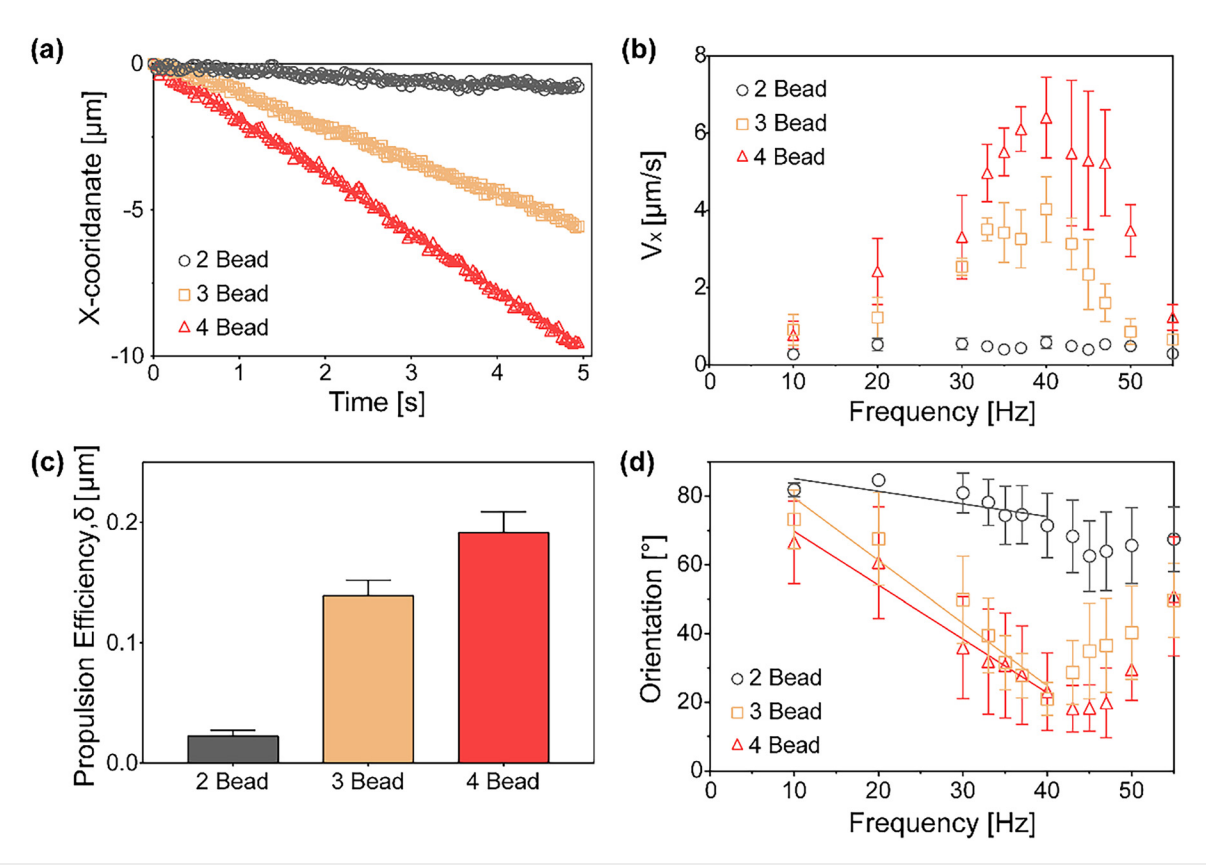


FIG. 2. Propulsion of self-assembled swimmers in water. (a) Plot showing the change in the swimmer x-co-ordinate at 40 Hz. (b) The velocity of all swimmers at discrete rotational frequencies. (c) Propulsion efficiency of swimmers at their step-out frequencies. (d) Orientation angle of swimmers as a function of frequency. n = 5.

one cyclic motion, achieved by normalizing the velocity by the step-out frequency, ω_{s-o} [Fig. 2(c)]. Similar to the results found in the displacement and velocity, the 4 bead swimmers maintain the highest propulsion efficiency followed by the 3 and 2 bead swimmers.

Another physical parameter extracted from the self-assembled magnetic swimmers is their orientation angles when actuated at a fixed frequency. After a critical frequency, the swimmers orient themselves with respect to the axis of rotation (x-axis) to minimize the magnetic energy, which we define as the orientation angle. We observe a decrease in the orientation angle as the frequency is increased. The rate of change of orientation, θ_{s-o}^- , until ω_{s-o} , is also found using linear curve fitting as shown in Fig. 2(d). The 3 bead swimmers have the highest rate followed by the 4 then 2 bead swimmers. Although the 3 bead swimmer starts at a higher averaged orientation than the 4 bead, at ω_{s-o} its orientation becomes similar to the 4 bead swimmer giving 3 bead swimmers a higher rate of decrease in orientation. The rate of change in the orientation angle, θ_{s-o}^+ , after ω_{s-o} , is positive for all self-assembled swimmers signifying that the orientation angle increases.

The magnetic swimmers dynamics in water will be used as a reference for the dynamics presented in the following sections. Overall the 4 bead swimmers have the highest velocity and propulsion efficiency. On the other hand, all swimmers decrease their orientation, and only the 3 and 4 bead swimmers reach \sim 22° at their $\omega_{s=0}$.

B. Self-assembled swimmers in xanthan gum

Six xanthan gum (XG) solutions are prepared following the protocol described in the methods section. The concentrations, c, chosen for the XG solutions range from 50 to 500 ppm, based on previous work which showed that viscoelastic effects are most dominant at low concentrations compared to higher polymer concentrations (c > 500 ppm) where viscous drag begins to dominate propulsion kinematics.²² The swimmers are actuated using a rotational magnetic field in the low concentration XG polymer fluids, and their propulsion kinematics are similar to that seen in water where all swimming regimes are observed. However, the range and magnitude of the magnetic driving frequencies decrease as the XG polymer concentration increases, see Figs. S2(a) and S2(b) in the supplementary material.

In the XG polymer fluids, the swimming velocity of all swimmers increases when increasing the rotational magnetic frequency. In the 50 ppm XG solution, 3 bead swimmers begin to have the highest propulsion velocity at 20 Hz compared to the other swimmer configurations and continues to maintain this trend until its step-out frequency is reached at 35 Hz [Fig. S2(a) in the supplementary material]. When the XG concentration is increased to 500 ppm, 2 bead self-assembled swimmers demonstrate high velocities compared to the 3 and 4 bead swimmers until the step-out frequency [Fig. S2(b) in supplementary material]. In all XG fluids, swimmers with the highest propulsion velocity at step-out frequency maintain the highest velocity after ω_{s-0}

until the asymmetrical rotation with the magnetic field eventually causes the velocities of the swimmers to become comparable. The change in orientation angle before the magnetic step-out frequency always decreases and is similar in all XG polymer fluid concentrations. However, the change in the swimmers orientation angles after the step-out frequency differs. In the 50 ppm XG fluid, the orientation angle begins to increase as $\omega > \omega_{s-o}$ while the opposite is seen in the 500 ppm XG fluid, where there is a continuous decrease in orientation angle [Figs. S2(c) and S2(d) in the supplementary material]. The transition of the orientation angle is characterized by its slope before θ_{s-o}^- and after θ_{s-o}^+ the step-out frequency. The θ_{s-o}^+ is the only parameter that changes with polymer concentration where the slope changes from positive to negative at different XG polymer concentrations signifying a continuous decrease in the orientation angle in XG concentrations greater than 300 ppm (data not shown).

To understand the dynamics of self-assembled swimmers, we compared the velocity ratio with respect to water at the same magnetic driving frequency. To estimate the velocity ratio, we assume that the velocity has a linear relationship with magnetic driving frequency in water, see Fig. 2(b). The magnetic frequency can also be defined by the dimensionless Deborah (De) number as the product of the angular frequency, Ω , and the relaxation time, τ . The relaxation time is determined from optical tweezer micro-rheology as it characterizes the fluids on a similar length-scale to the self-assembled magnetic microswimmers. Briefly, the polymer fluids are seeded with 1 μ m spherical probes and enclosed by a coverslip, glass slide, and spacer (see methods). After calibrating the optical system, ²⁵ the probes are trapped

with a laser power of 10 mW and oscillated at varying frequencies to determine the storage and loss modulus. From the loss modulus, the imaginary complex viscosity is found as a function of frequency, which is then fit with a multi-mode generalized linear viscoelastic model [Eq. (1)]. XG fluids are fit with n = 2, except the 50 ppm, which shows good agreement with n = 1. The averaged relaxation times on the order of increasing concentrations are 2.0, 39.1, 31.0, 32,1, 36.1, and 52.3 ms, respectively. For 2 bead swimmers, an increasing velocity ratio with driving frequency is observed. The increase is illuminated when graphed with respect to the De number, identifying two trends when De < 1 and De > 1 [Fig. 3(a)]. For 3 bead swimmers, while the velocity ratio appears to decrease with increasing frequency, when represented by the De number, the 50 ppm data shifts revealing an increase in the velocity ratio with De [Fig. 3(b)]. Finally, 4 bead swimmers always show a decreasing velocity ratio compared to both frequency [Fig. 3(c)] and De number.

The dynamics previously shown compares swimmers at similar frequencies, next we focus on the velocity ratio at the step-out frequency, which corresponds to the frequency that gives the highest propulsion velocity. These parameters are graphed as a function of polymer concentration normalized by concentration at which the polymer-polymer interactions become important known as the overlap concentration, c* [Figs. 3(d) and 3(e)]. The 2 bead swimmers' average velocity substantially increases when placed in 50 ppm XG (0.05 c/c*) compared to their dynamics in water. This increasing velocity reaches its maximum in the 100 ppm XG (0.11 c/c*) solution, achieving an average velocity of 6.51 μ m/s. This significant increase in the

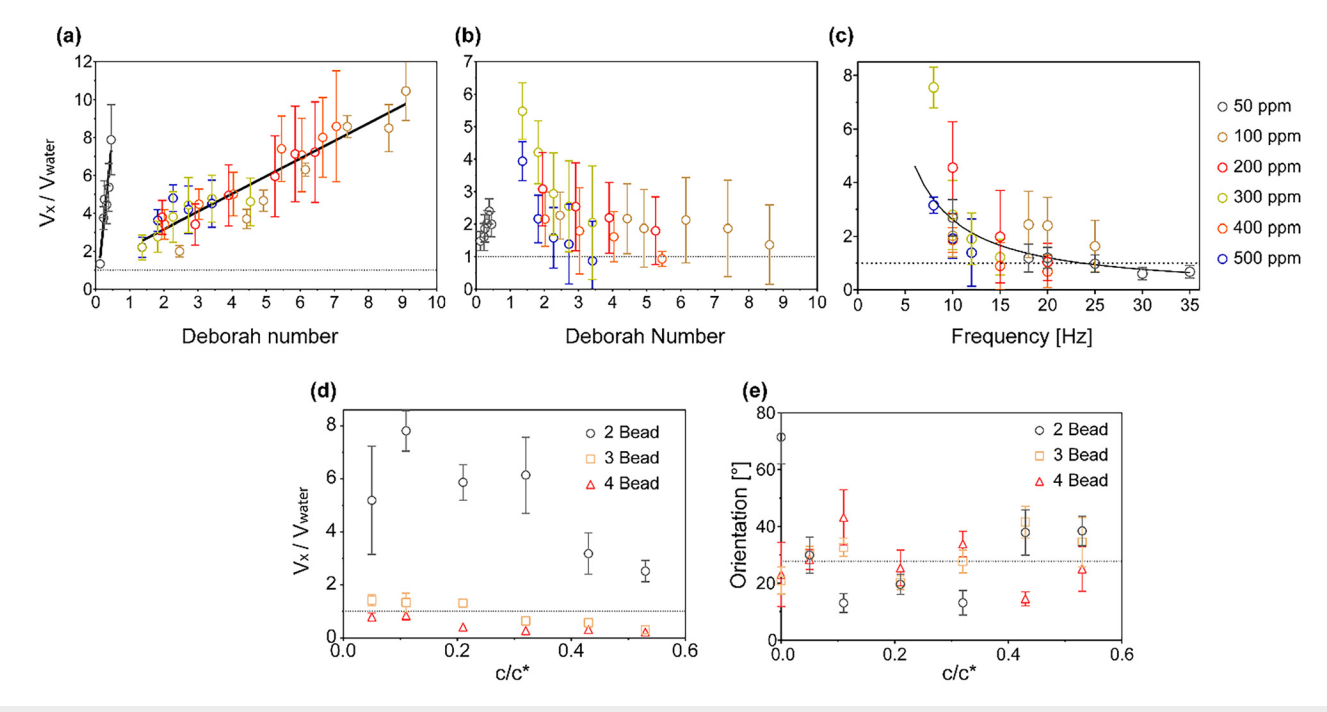


FIG. 3. Normalized swimming velocity and orientation angles in dilute xanthan gum solutions. Velocity ratio of (a) 2 bead and (b) 3 bead swimmers at similar frequencies as a function of Deborah number. (c) The velocity ratio of 4 bead swimmers at similar frequencies as a function of the magnetic driving frequency. Black solid lines identify trends for the velocity ratio. (d) The velocity ratio of the self-assembled magnetic swimmers at their step-out frequency. Dashed lines at y = 1 represent the normalized velocity in water. (e) Orientation angles of the magnetic swimmers at their step-out frequency in varying concentrations of xanthan gum (c* \sim 950 ppm). The dashed line represents the average orientation angle at 27.7°, excluding the orientation angle of 2 bead swimmers in water.

velocity ratio in XG fluids captures the 2 bead swimmers' inability to propel in Newtonian fluids due to its symmetry. Further increase in the XG polymer concentration results in the reduction of the 2 beads' velocity, which still retains a higher velocity when compared to water. When the number of beads forming a swimmer increases from two to three, the velocity is also seen to increase slightly compared to the propulsion dynamics in water. The 3 bead swimmer reaches its maximum velocity in the 50 ppm XG solution. However, the 3 bead swimmer's velocity eventually decreases compared to water when the polymer concentration is greater than 300 ppm $(0.32 c/c^*)$. On the other hand, the 4 bead's propulsion velocity continuously decreases as the polymer concentration is increased, deviating from 2 and 3 bead swimmers. Despite the variation in swimming velocity, their swimming gait quantified by the orientation angle at their step-out frequency remains relatively constant at 27.7° excluding the orientation angle of the 2 bead swimmers in water.

C. Self-assembled swimmers in λ -DNA

We further explored the effect of shear-thinning viscosity on the self-assembled magnetic microswimmers using another well-characterized shear-thinning fluid, λ -DNA. Here, the three swimming regimes are also observed, and similar to the dynamics in water the 4 bead configuration always has the highest velocity followed by 3 and 2 bead swimmers. The evolution of the orientation angle also follows similar dynamics to water where the rate of change of the orientation

angle decreases and increases, before and after the step-out frequency for all DNA concentrations. When the velocity ratio is compared to the magnetic driving frequency at similar frequencies in DNA fluids, it fluctuates steadily about $V_x/V_{x,water}=1$, indicating that the dynamics are analogous to a Newtonian solvent. However, in 20 ppm DNA the velocity ratio for 2 bead swimmers shows a linear increasing trend while 3 and 4 bead swimmers show a non-linear decrease. The relaxation time for the 20 ppm DNA solution best fits with n=2 using the multi-mode generalized linear viscoelastic model resulting in an average relaxation time of 126.1 ms. Hence, swimmers in the 20 ppm DNA fluid are propelled in shear-thinning fluids where elastic effects become important (De > 1).

At the step-out frequency, all self-assembled magnetic microswimmers' velocity decreases when compared to their velocity in water [Fig. 4(a)]. Overall, similar to the kinematics in XG, the 4 bead swimmers decrease their average propulsion velocity as the DNA concentration increases. On the other hand, while the 3 bead swimmers velocity decreases, they maintain a nearly average velocity despite the polymer fluid's concentration where it eventually has similar translational velocity ratio to the 4 bead swimmer at a DNA concentration of 20 ppm $(0.5\,c/c^*)$. The decrease in the velocity ratio for 3 and 4 bead swimmers at their step-out frequency is a result of them propelling in a shear-thinning fluid with elasticity. The 2 bead swimmers, however, maintain similar dynamics to that seen in water until the velocity doubles when being actuated in the 20 ppm $(0.5\,c/c^*)$ DNA fluid, see Fig. 4(c) (Multimedia view), due to 2 bead swimmers ability to propel in

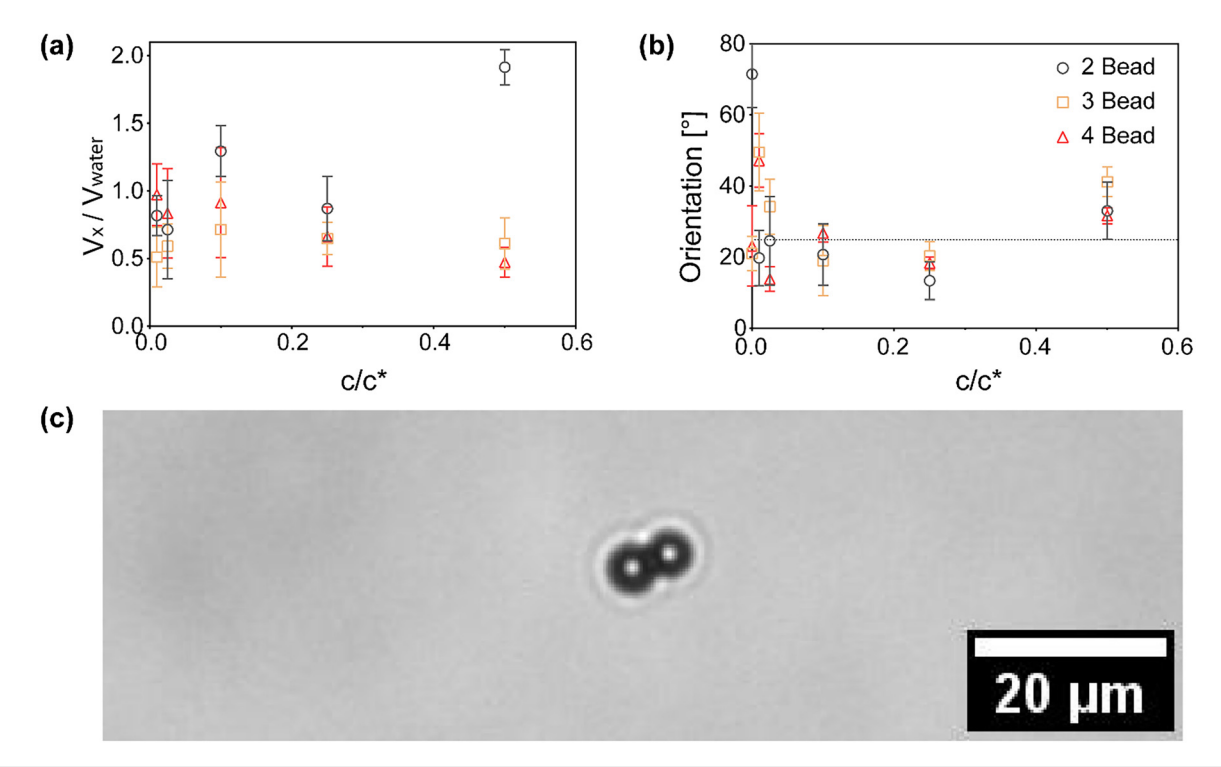


FIG. 4. Normalized swimming velocity compared to water in λ -DNA solutions. (a) Velocity ratio compared to water and (b) orientation angles of the magnetic swimmers at their step-out frequencies in varying concentrations of λ -DNA. $c^* \sim 40$ ppm. The dashed line represents the average orientation angle at 24.9° excluding the orientation angle of 2 bead swimmers in water. (c) Still image of a rigid 2 bead microswimmer being actuated in 20 ppm λ -DNA using a homogeneous, rotational magnetic field at varying driving frequencies. Multimedia available online.

shear-thinning fluids with or without elasticity. Similar to XG, when the 2 bead swimmers are placed in the DNA polymer fluid, their orientation angles at step-out frequency, decreases greatly [Fig. 4(b)]. However, no significant trends are identified for all swimmers with an average orientation of 24.9° , excluding the orientation angle of 2 bead swimmers in water.

IV. DISCUSSION

Viscoelastic effects are known to modify the kinematics of self-assembled, magnetically actuated microswimmers. 10,26 In polymer fluids, such as methyl cellulose and polyacrylamide, 4 bead swimmers maintain a higher velocity and propulsion efficiency than 3 bead swimmers. However, this trend is inverted when placed in the shear-thinning viscosity polymer, such as xanthan gum. 22 Here, we focus on why fluids exhibiting shear-thinning viscosity alter the kinematics of these self-assembled swimmers using two polymer fluids, xanthan gum, and λ -DNA. All swimmers are actuated in polymer fluids below their overlap concentration, and concentrations are chosen where viscoelastic effects can be distinguished from linear fluidic drag. Hence, the change in dynamics exhibited by the microswimmers can be due to a change in their swimming gait, a fluidic response to being sheared, or a coupling of both effects.

In the propulsion regime, the self-assembled swimmers orient themselves due to their magnetization axis and are able to produce rotational anisotropy to translate. In both XG and DNA polymer fluids, no significant change in orientation angle is observed when compared to swimming in water except for the 2 bead swimmers. Hence, swimmers achieve their maximum velocity in their respective fluids when oriented between 20° and 35°. Another physical parameter is the arc angle, which describes the geometrical angle of the selfassembled magnetic swimmers. For instance, the 2 bead swimmers always have an arc angle of 180°; however, as more beads are added, swimmers geometry begins to form an arc (Fig. 1). While there is variation in the arc angle due to the self-assembled nature of swimmers, we note that the arc angle varies between 100 and 150° and, in other viscoelastic fluids, 4 bead swimmers still maintained the highest propulsion velocity.²² Therefore, we observe no change in the physical parameters of the rigid swimmers to explain the effect of shearthinning viscosity.

We next observed the velocity ratio of self-assembled magnetic swimmers at the same frequency using the dimensionless Deborah (De) number. At similar frequencies, distinct dynamics are observed when the polymeric fluid has (1) no shear-thinning, (2) shear-thinning with negligible elasticity (De < 1), and (3) shear-thinning with elasticity (De > 1). With no shear-thinning properties, all swimmers maintain dynamics similar to when in water, seen in the λ -DNA polymer solutions when $c \le 10$ ppm resulting in 2, 3, and 4 bead swimmers having a constant velocity ratio. We note that microrheology revels no change in viscosity when $c \le 10$ ppm for DNA solutions causing 2 bead swimmers to remain inefficient propellers and 3 bead swimmers maintaining similar velocities. Only 4 bead swimmers show a decrease in velocity with increasing DNA concentration due to hydrodynamic drag.

A. Shear-thinning fluids with negligible elasticity

When shear-thinning viscosity is present and there is negligible elasticity (De < 1), propulsion kinematics are dependent on the

geometry of the swimmer. In 50 ppm XG, 3 bead swimmers have higher velocities than 4 bead swimmers [Fig. S2(a) in supplementary material], and only 2 and 3 bead swimmers show enhanced swimming velocity ratios with frequency, leading to them having a higher velocity than in water at their step-out frequencies [Fig. 3(d)]. While 2 bead swimmers are inefficient in water, 3 bead swimmers can propel in water due to pseudo-chirality; despite this fact, 3 bead swimmers velocity show increased swimming enhancement in 50 ppm. Conversely, 4 bead swimmers constantly decrease their velocity ratio as the frequency increases, resulting in a velocity ratio below one at the step-out frequency.

For small De number (De < 1), Eberhard et al. used an oscillating 2 bead swimmer to show that propulsion is achieved as the viscoelasticity breaks the symmetry during a cycle.²⁷ The authors further stated as the geometry of the beads became similar the viscoelasticity effect diminishes, resulting in no propulsion. Another explanation for swimmers in shear-thinning fluids with negligible elasticity focuses on the actuation of a large amplitude sheet that can increase swimmer velocity.²⁸ This phenomenon is caused by the fluid viscosity being low near the sheet but increases to the zero-shear viscosity away from the swimmer akin to swimming between two walls. We hypothesize, in a shear-thinning fluid with negligible elasticity, 2 and 3 bead swimmers experience the confinement effect.²⁹ On the other hand, 4 bead swimmers' large geometry dissipates their confinement resulting in a viscosity gradient similar to a Newtonian solvent; hence, only hydrodynamics drag is experienced. Therefore, the drag anisotropy from a tightly attached confinement³⁰ causes the 2 and 3 bead swimmers to substantially increase their propulsion velocity.

B. Shear-thinning fluids with elasticity

Next, the shear-thinning fluid can display elastic (De > 1) properties, which also affects the swimmer dynamics based on the swimmer configuration as a result of flow asymmetry.³¹ In this region, 2 bead swimmers show increasing velocity ratio with frequency, while 3 and 4 bead swimmers velocity ratio decreases with the driving frequency. To provide further insight, we use co-moving frame PIV to compare the flow fields of the self-assembled magnetic swimmers in water and 200 ppm XG at 30 Hz (De \sim 5.6). Briefly, the fluids are seeded with 500 nm tracer particles to attain a 0.025% w/v solution and are then mixed with the self-assembled magnetic swimmers. Experimental chambers are prepared similar to the schematic in Fig. 1 and, swimmers are made of two to four magnetic beads and actuated using a homogeneous rotational magnetic field. Here, co-moving frame PIV is performed by tracking the centroid of the swimmer, then cropping 100 pixels (\sim 30 μ m) from the centroid and reconstructing the video to give the appearance of a stationary swimmer unless otherwise stated. Although the tracers do not modify the observed kinematics of the magnetic swimmers, in a viscoelastic fluid particle migration can exist within the viscosity or shear rate gradient of the swimmer. In water, the flow travels perpendicular to the axis of rotation as a result of the rotational motion of the swimmers. The dynamics of driven rotational magnetic microswimmers are known to generate rotational motion in Newtonian fluids³² [Figs. 5(a), 5(c), and S3(a) in supplementary material]. However, in the 200 ppm XG fluid, the flow around the swimmer's body experiences rotational motion, while the fore and aft flow moves parallel to the rotational axis of the swimmer, similar to that of a source at both ends, as seen in Figs. 5(b), 5(d) and S3(b) in

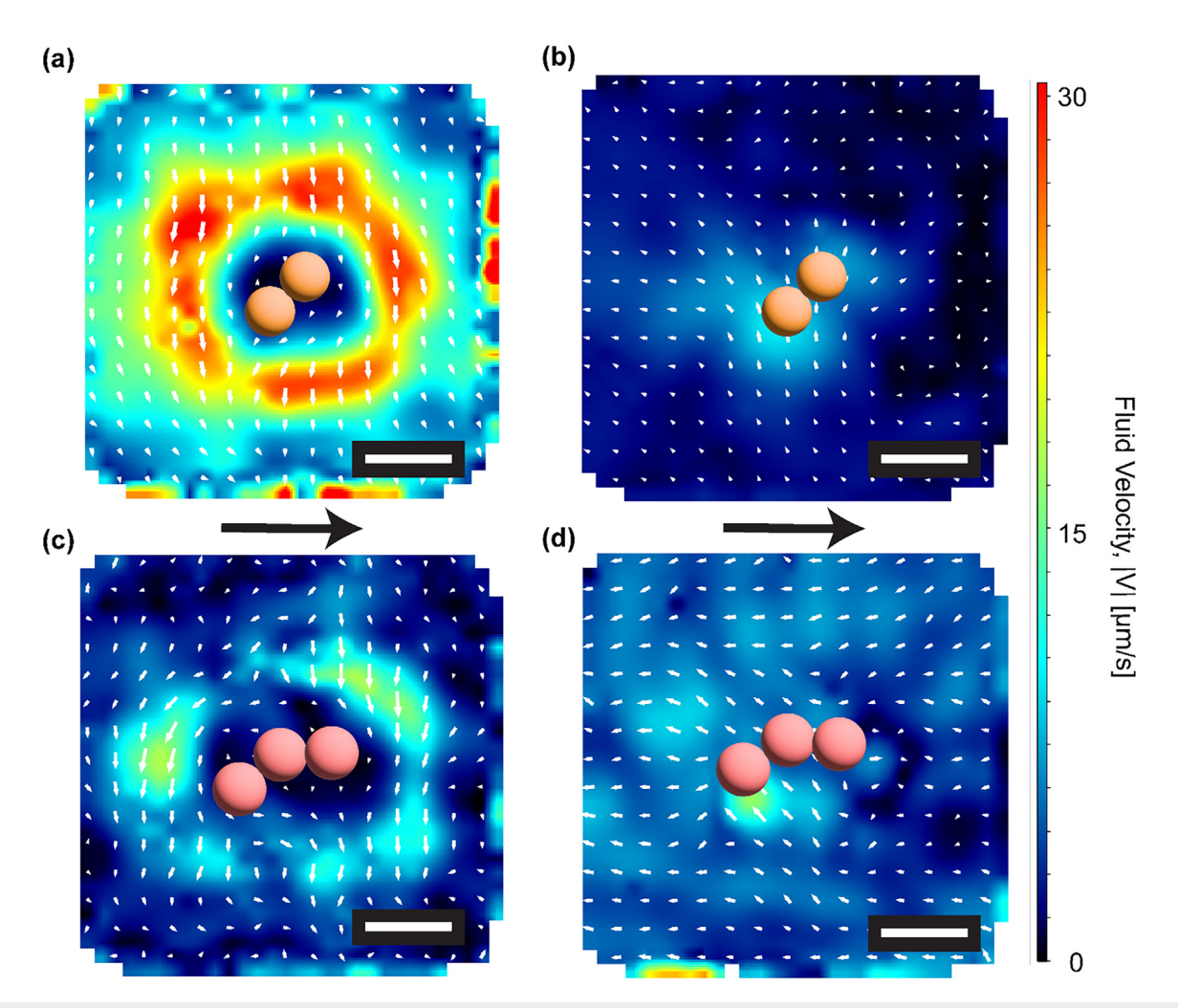


FIG. 5. Time-averaged 2D flow fields of self-assembled 2 and 3 bead magnetic swimmers rotated at 30 Hz in (a) and (c) water and (b) and (d) 200 ppm xanthan gum. Scale = 10 μ m. The black arrows at the center of the figures (a) and (c) or (b) and (d) indicate the swimming direction for the self-assembled magnetic swimmers.

supplementary material. Hence, the fluid dynamics in XG is akin to elastic effects where the curved streamlines generate hoop stresses resulting in secondary flows^{18,19} parallel to the axis of rotation.

We next compare the magnitude of the flow field's velocity for the self-assembled magnetic swimmers. In the Newtonian solvent, flows produced around swimmers are purely rotational and of equal magnitude in the transverse direction, perpendicular to the axis of rotation. In the axial direction, only the 3 and 4 bead swimmers have an asymmetry between the magnitude of the fore-aft rotational flow velocity while the 2 bead's flow field is symmetric (Fig. S4 in supplementary material). In 200 ppm XG, the flow is purely rotational along the transverse direction but changes from rotational to lateral flow with unequal flow field magnitudes at opposite ends of swimmers.

For swimmers in shear-thinning fluids, as the fluid elasticity increases through either polymer concentration or magnetic driving frequency resulting in the local stretching of polymer molecules, we propose that the Weissenberg (rod climbing) effect dominates swimming kinematics. These effects result from the

polymer macromolecule stretching along the swimmer's body and then contracting at the swimmer's end, creating secondary flows similar to an elastic jet. 33,34 At low De (\sim 1), 2 bead swimmers are not expected to propel as the elastic forces cancel due to symmetry; 19 however, we observe propulsion due to spontaneous symmetry breaking of the fluid, 18 which can be caused by the minor differences in the magnetic beads diameter. The enhancement of the elastic jet by increasing elasticity hinders the dynamics for 3 ($c \ge 300 \, \text{ppm XG}$) and 4 bead swimmers due to the reduction of fluid forces.^{35–37} The PIV experiments also show that 3 and 4 bead swimmers produce elongational stresses against the swimmer propulsion direction adding resistance to the flow. 38 While hydrodynamic drag plays a significant role in the swimmer kinematics, in our system we observe the velocity ratio as a function of frequency follows an exponential decay; therefore, viscoelastic effects also contribute to swimmer dynamics. Similar dynamics are seen for biological organisms, 39,40 which possess a finite energy source, attributing their decreased propulsion in elastic fluids to the

extra elastic stresses, which add resistance and change their swimming gait.

V. CONCLUSION

The locomotion of non-helical, self-assembled swimmers actuated by a rotational magnetic field has been previously shown to be affected by local viscoelastic effects. Here, we focus on how the propulsion kinematics of driven self-assembled swimmers made of 2–4 magnetic beads is affected in model shear-thinning viscosity polymer fluids, xanthan gum, and λ -DNA. Microswimmers are actuated at varying frequencies and the swimmers' swimming velocity and orientation angle are recorded. The velocity ratio of the swimmers at similar frequencies and step-out frequencies is shown to be greatly affected by the introduction of the shear-thinning polymer molecules unlike the orientation angle, which remains relatively constant.

We characterize our fluids and distinguish among them by (1) no shear-thinning, (2) shear-thinning with negligible elasticity, and (3) shear-thinning with elasticity. When there is no shear-thinning, swimmers only experience the fluid's hydrodynamic drag, causing their velocity to decrease. In a shear-thinning fluid with negligible elasticity, only 2 and 3 bead swimmers show enhanced propulsion, which we attribute to the confinement effect. On the other hand, 4 bead swimmers' size causes a viscosity gradient similar to a Newtonian fluid, preventing them from being influenced by the confinement effect. Finally, in a shear-thinning fluid with elasticity, the Weissenberg effect allows 2 bead swimmers to increase their propulsion due to the spontaneous breaking of the symmetry, 3 bead swimmers to maintain similar velocities as water, and 4 bead swimmers dynamics are hindered due to the elastic stresses adding resistance. Hence, 2 bead swimmers show swimming enhancement in both XG and λ -DNA polymer fluids while the 3 bead swimmer only shows enhancement in XG fluids. Although 4 bead swimmers propel in water, their velocities are shown to constantly decrease with increasing polymer concentration regardless of the fluids shear-thinning properties. We use particle image velocimetry to visualize the fluid flow produced by the self-assembled swimmers in both water and 200 ppm XG. We note that for propulsion of self-assembled microswimmers, it is necessary to have flow asymmetry, which can be created in a shear-thinning fluid with and without elasticity.

Although we are able to show how shear-thinning viscosity can enhance or attenuate self-assembled swimmer locomotion, more work is needed to understand why swimmers are affected in distinct ways. Hence, future work should focus on observing the flow fields for distinct geometries defined by the arc angle, made of a fixed number of beads in viscoelastic and Newtonian fluids of similar viscosities at varying magnetic field strengths and frequencies. In addition, normal stress differences should be accounted for in elastic fluids and what additional effects arise when further increasing the elasticity of the fluid.

SUPPLEMENTARY MATERIAL

See the supplementary material for additional experimental data characterizing fluid properties, swimming kinematics and extended PIV plots.

ACKNOWLEDGMENTS

This work was funded by the National Science Foundation (Grant Nos. HDR-2000202 and CMMI-2000330) and supported by the NSF FAMU CREST Center award (Grant No. HDR-1735968).

This research work was also supported by The Grainger Foundation Frontiers of Engineering Grant under the National Academy of Sciences Award No.: 2000013181. This material is based upon work supported by the Air Force Office of Scientific Research under Award No. FA9550-22-1-0247. All the work was performed at the National High Magnetic Field Laboratory, which is supported by National Science Foundation Cooperative Agreement No. DMR-1644779 and the State of Florida.

The content is solely the responsibility of the authors and does not necessarily represent the official views of The Grainger Foundation or the National Academy of Sciences.

AUTHOR DECLARATIONS Conflict of Interest

The authors have no conflicts to disclose.

Author Contributions

David Quashie Jr.: Conceptualization (equal); Data curation (lead); Formal analysis (lead); Visualization (lead); Writing – original draft (lead); Writing – review & editing (lead). Qi Wang: Writing – original draft (supporting); Writing – review & editing (supporting). Sophie Jermyn: Writing – original draft (supporting); Writing – review & editing (supporting). Jaideep Katuri: Writing – original draft (supporting); Writing – review & editing (supporting). Jamel Ali: Conceptualization (equal); Funding acquisition (lead); Project administration (lead); Supervision (lead); Writing – original draft (supporting); Writing – review & editing (supporting).

DATA AVAILABILITY

The data that support the findings of this study are available from the corresponding author upon reasonable request.

REFERENCES

- ¹F. Wei, T. Zhong, Z. Zhan, and L. Yao, "Self-assembled micro-nanorobots: From assembly mechanisms to applications," ChemNanoMat 7, 238 (2021).
- ²D. Schamel, A. G. Mark, J. G. Gibbs, C. Miksch, K. I. Morozov, A. M. Leshansky, and P. Fischer, "Nanopropellers and their actuation in complex viscoelastic media," ACS Nano 8, 8794 (2014).
- ³V. Angeles, F. A. Godínez, J. A. Puente-Velazquez, R. Mendez-Rojano, E. Lauga, and R. Zenit, "Front-back asymmetry controls the impact of viscoelasticity on helical swimming," Phys. Rev. Fluids **6**, 043102 (2021).
- ⁴M. A. Joens, P. S. Doyle, G. H. McKinley, and J. W. Swan, "Time-dependent two-dimensional translation of a freely rotating sphere in a viscoelastic fluid," Phys. Fluids **34**, 123110 (2022).
- ⁵P. J. Vach, P. Fratzl, S. Klumpp, and D. Faivre, "Fast magnetic micropropellers with random shapes," Nano Lett. 15, 7064 (2015).
- ⁶G. Go, J. Han, J. Zhen, S. Zheng, A. Yoo, M.-J. Jeon, J.-O. Park, and S. Park, "A magnetically actuated microscaffold containing mesenchymal stem cells for articular cartilage repair," Adv. Healthcare Mater. 6, 1601378 (2017).
- ⁷A. Aghakhani, O. Yasa, P. Wrede, and M. Sitti, "Acoustically powered surface-slipping mobile microrobots," Proc. Natl. Acad. Sci. U. S. A. 117, 3469 (2020).
- ⁸J. G. Lee, A. M. Brooks, W. A. Shelton, K. J. M. Bishop, and B. Bharti, "Directed propulsion of spherical particles along three dimensional helical trajectories," Nat. Commun. 10, 2575 (2019).
- ⁹A. Al Harraq, M. Bello, and B. Bharti, "A guide to design the trajectory of active particles: From fundamentals to applications," Curr. Opin. Colloid Interface Sci. 61, 101612 (2022).

- ¹⁰J. Ignés-Mullol and F. Sagués, "Experiments with active and driven synthetic colloids in complex fluids," Curr. Opin. Colloid Interface Sci. 62, 101636 (2022).
- ¹¹U. K. Cheang, F. Meshkati, D. Kim, M. J. Kim, and H. C. Fu, "Minimal geometric requirements for micropropulsion via magnetic rotation," Phys. Rev. E **90**, 033007 (2014)
- ¹²Z. Chen, Z. Wang, D. Quashie, P. Benhal, J. Ali, M. J. Kim, and U. K. Cheang, "Propulsion of magnetically actuated achiral planar microswimmers in Newtonian and non-Newtonian fluids," Sci. Rep. 11, 21190 (2021).
- ¹³F. Meshkati and H. C. Fu, "Modeling rigid magnetically rotated microswimmers: Rotation axes, bistability, and controllability," Phys. Rev. E 90, 063006 (2014).
- ¹⁴K. I. Morozov, Y. Mirzae, O. Kenneth, and A. M. Leshansky, "Dynamics of arbitrary shaped propellers driven by a rotating magnetic field," Phys. Rev. Fluids 2, 044202 (2017).
- ¹⁵L. Y. Tan, J. Ali, U. K. Cheang, X. C. Shi, D. Kim, and M. J. Kim, "µ-PIV measurements of flows generated by photolithography-fabricated achiral microswimmers," Micromachines 10, 865 (2019).
- ¹⁶Q. Wang, L. Yang, J. Yu, and L. Zhang, "Characterizing dynamic behaviors of three-particle paramagnetic microswimmer near a solid surface," Rob. Biomimetics 4, 20 (2017).
- ¹⁷P. Tierno, R. Golestanian, I. Pagonabarraga, and F. Sagués, "Controlled swimming in confined fluids of magnetically actuated colloidal rotors," Phys. Rev. Lett. 101, 218304 (2008).
- ¹⁸L. W. Rogowski, J. Ali, X. Zhang, J. N. Wilking, H. C. Fu, and M. J. Kim, "Symmetry breaking propulsion of magnetic microspheres in nonlinearly viscoelastic fluids," Nat. Commun. 12, 1116 (2021).
- ¹⁹J. A. Puente-Velázquez, F. A. Godínez, E. Lauga, and R. Zenit, "Viscoelastic propulsion of a rotating dumbbell," Microfluid. Nanofluid. 23, 108 (2019).
- ²⁰N. C. Keim, M. Garcia, and P. E. Arratia, "Fluid elasticity can enable propulsion at low Reynolds number," Phys. Fluids 24, 081703 (2012).
- ²¹P. Benhal, D. Quashie, U. K. Cheang, and J. Ali, "Propulsion kinematics of achiral microswimmers in viscous fluids," Appl. Phys. Lett. 118, 204103 (2021).
- ²²D. Quashie, Jr., D. Gordon, P. Nielsen, S. Kelley, S. Jermyn, and J. Ali, "Propulsion efficiency of achiral microswimmers in viscoelastic polymer fluids," AIChE J. 69, e17988 (2023).
- ²³J. S. Hur, E. S. G. Shaqfeh, H. P. Babcock, D. E. Smith, and S. Chu, "Dynamics of dilute and semidilute DNA solutions in the start-up of shear flow," J. Rheol.
- ²⁴H. Seyforth, M. Gomez, W. B. Rogers, J. L. Ross, and W. W. Ahmed, "Nonequilibrium fluctuations and nonlinear response of an active bath," Phys. Rev. Res. 4, 023043 (2022).

- ²⁵F. Català-Castro, V. Venturini, S. Ortiz-Vásquez, V. Ruprecht, and M. Krieg, "Direct force measurements of subcellular mechanics in confinement using optical tweezers," JoVE 174, e62865 (2021).
- ²⁶ A. E. Patteson, A. Gopinath, and P. E. Arratia, "Active colloids in complex fluids," Curr. Opin. Colloid Interface Sci. 21, 86 (2016).
- 27 M. Eberhard, A. Choudhary, and H. Stark, "Why the reciprocal two-sphere swimmer moves in a viscoelastic environment," Phys. Fluids 35, 063119 (2023)
- ²⁸G. Li and A. M. Ardekani, "Undulatory swimming in non-Newtonian fluids," J. Fluid Mech. **784**, R4 (2015).
- 29S. Gómez, F. A. Godínez, E. Lauga, and R. Zenit, "Helical propulsion in shear-thinning fluids," J. Fluid Mech. 812, R3 (2017).
- 30E. Demir, N. Lordi, Y. Ding, and O. S. Pak, "Nonlocal shear-thinning effects substantially enhance helical propulsion," Phys. Rev. Fluids 5, 111301 (2020)
- ³¹S. Varchanis, C. C. Hopkins, A. Q. Shen, J. Tsamopoulos, and S. J. Haward, "Asymmetric flows of complex fluids past confined cylinders: A comprehensive numerical study with experimental validation," Phys. Fluids 32, 053103 (2020).
- ³²M. Pal, I. Fouxon, A. M. Leshansky, and A. Ghosh, "Fluid flow induced by helical microswimmers in bulk and near walls," Phys. Rev. Res. 4, 033069 (2022).
- ⁵³L. A. Kroo, J. P. Binagia, N. Eckman, M. Prakash, and E. S. G. Shaqfeh, "A freely suspended robotic swimmer propelled by viscoelastic normal stresses," J. Fluid Mech. 944, A20 (2022).
- 34Y.-G. Irilan and F. R. Cunha, "Experimental and theoretical studies of the fluid elasticity on the motion of macroscopic models of active helical swimmers," Phys. Fluids 34, 053103 (2022).
- 35G. Li, E. Lauga, and A. M. Ardekani, "Microswimming in viscoelastic fluids," J. Non-Newtonian Fluid Mech. 297, 104655 (2021).
- ³⁶C. Datt, L. Zhu, G. J. Elfring, and O. S. Pak, "Squirming through shear-thinning fluids," J. Fluid Mech. **784**, R1 (2015).
- 37B. van Gogh, E. Demir, D. Palaniappan, and O. S. Pak, "The effect of particle geometry on squirming through a shear-thinning fluid," J. Fluid Mech. 938, A3 (2022).
- ³⁸L. Zhu, E. Lauga, and L. Brandt, "Self-propulsion in viscoelastic fluids: Pushers vs. pullers," Phys. Fluids 24, 051902 (2012).
- 39T. D. Montenegro-Johnson, D. A. Gagnon, P. E. Arratia, and E. Lauga, "Flow analysis of the low Reynolds number swimmer C. elegans," Phys. Rev. Fluids 1, 053203 (2016)
- 40B. Qin, A. Gopinath, J. Yang, J. P. Gollub, and P. E. Arratia, "Flagellar kinematics and swimming of algal cells in viscoelastic fluids," Sci. Rep. 5, 9190 (2015)